Applied Surface Science 605 (2022) 154677

Contents lists available at ScienceDirect

Applied Surface Science

journal homepage: www.elsevier.com/locate/apsusc

Full length article

Texture in ITO films deposited at oblique incidence by ion beam sputtering

Bertrand Lacroix [a,b,*], Fabien Paumier [c], Antonio J. Santos [a,b], Florian Maudet [c], Thierry Girardeau [c], Cyril Dupeyrat [d], Rafael García [a,b], Francisco M. Morales [a,b]

[a] Department of Materials Science and Metallurgic Engineering, and Inorganic Chemistry, University of Cádiz, 11510 Puerto Real, Spain
[b] IMEYMAT: Institute of Research on Electron Microscopy and Materials, University of Cádiz, 11510 Puerto Real, Spain
[c] Institut Pprime, UPR 3346 CNRS-Université de Poitiers-ENSMA, SP2MI, 86962 Futuroscope-Chasseneuil Cedex, France
[d] Safran Electronics & Defense, 26 Avenue des Hauts de la Chaume, 86280 Saint-Benoît, France

ARTICLE INFO

Keywords:
Indium tin oxide
Ion beam sputtering
Oblique angle deposition
Thin films
Texture
Morphology

ABSTRACT

Texture of crystalline In_2O_3:Sn (ITO) thin films prepared by combining ion beam sputtering (IBS) at room temperature and oblique angle deposition (OAD) has been studied depending on the vapor incidence on Si substrates (α, ranging from 50° to 85°) and the ions used to sputter the target (argon or xenon accelerated at 1.2 keV). Films obtained using Xe ions show an unusual evolution depending on the deposition angle α, with the development of a dual biaxial (1 1 1) off-axis texture for $\alpha \leq 70°$, and a switching in the preferred out-of-plane orientation from [1 1 1] to [0 0 1] for $\alpha > 70°$ that leads to a biaxial (0 0 1) texture at highest deposition angles. These behaviors are well described by mechanisms involving a maximization of the direct capture of the adatoms on {1 1 1} planes, which can however be hindered when mobilities are exalted such as in the case of Ar deposition. The tuning of adatoms mobilities through the IBS process mixed with the control of the deposition angle offered by the OAD geometry appears as an efficient route to achieve an upgraded texture engineering in nanostructured ITO thin films.

1. Introduction

The development of preferred crystallographic orientations is an important aspect to take into account when dealing with crystalline thin films since it can strongly influence their properties, performance and reliability [1]. Several works have in fact shown that the fabrication of textured coatings may or may not be beneficial, depending on the targeted applications such as contacts and interconnects in microelectronics [2–4], optical coatings [5,6], wear protections [7], high-temperature superconductors [8–10], gas sensing devices [11,12] or conversion material electrodes for batteries [13]. However, this facet of thin films being far from straightforward, the mechanisms that drive the texture formation are often misunderstood or even overlooked. Dedicated thorough studies like the one proposed in this paper become therefore essential to better know the influence of key manufacturing parameters involved during deposition and eventual post-deposition processes, in order to achieve an ultimate control of the performances towards technological applications.

In the past decades, extensive research has been devoted to assess how texture develops in thin films and to find ways to tailor it. Ion beam bombardment during the films growth has for example been found to have a pronounced effect due to ion channeling and preferential sputtering effects [14–18]. Oblique angle deposition (OAD), generally combined with physical vapor deposition (PVD) processes like evaporation or magnetron sputtering, is another attractive route that relies in adjusting the direction of the incoming species onto the substrate. Indeed, besides providing films with controlled porosity and made of singular nanostructures in the form of tilted and separated nanocolumns (essentially due to shadowing effects), OAD offers an additional variable to control the texture as compared to conventional depositions at normal incidence, allowing the development of preferred orientations both perpendicularly (out-of-plane orientation) and parallel (in-plane orientation) to the surface of the film. Although texture evolutions in OAD films have already been widely reported for pure metals (Cr, Ru, Ti, Mo, Mg, W) [19–24] and metal nitrides (TiN, TiAlN, HfN, ZrN) [19,25,26], it still remains relatively under-explored in metal oxide films, with only a few studies on YBCO, YSZ and MgO mainly [19,27–29].

In this paper, particular attention will be paid on the texture build-up and control in nanostructured films of indium tin oxide (In_2O_3:Sn or ITO). Because of its high electrical conductivity and optical transparency, ITO has been one of the most widely studied transparent

* Corresponding author at: Department of Materials Science and Metallurgic Engineering, and Inorganic Chemistry, University of Cádiz, 11510 Puerto Real, Spain.
E-mail address: bertrand.lacroix@uca.es (B. Lacroix).

https://doi.org/10.1016/j.apsusc.2022.154677
Received 22 May 2022; Received in revised form 29 July 2022; Accepted 24 August 2022
Available online 27 August 2022

conducting oxides (TCOs). TCOs – including ITO, ZnO, SnO_2 and their doped counterparts – are essential for many optoelectronic applications such as flat panel displays, solar cells and electroluminescent devices as transparent electrode [30]. In TCOs prepared as dense coatings, texture can play a major role on their properties (in particular on electrical performances) and clear correlations with the film deposition conditions and properties have been reported in the literature [31–36]. For example, (2 1 1) ITO films prepared by DC magnetron sputtering were found clearly less conducting than (2 2 2)-textured ones [31]. Other work pointed out that the resistivity of fluorine-doped tin oxide films increases with strengthening the [1 1 0] orientation and weakening [2 0 0] [36]. However, to the best of our knowledge, only a few studies attempt to clarify the underlying texturing mechanisms in TCOs films and very few approaches to tailor the crystalline texture are reported [37–40]. In the particular case of dense ITO films, a switching from a (2 1 1) to (4 0 0) and (4 1 1) preferred growth has been reported using magnetron sputtering either in RF or DC modes [32]. Playing with the deposition atmosphere and energy of impinging particles during the growth of ITO by magnetron sputtering is also effective to set the preferred orientation: (2 1 1) films with superior properties have for instance been prepared at high sputtering power and low working pressure in a weak reducing ambient [41]. Surface morphology and grain orientation can also be effectively controlled by metal–organic chemical vapor deposition (MOCVD) through the temperature and growth rate [40]. In addition, ion-beam-assisted deposition (IBAD) at room temperature allows the formation of biaxially-textured ITO thin films with improved electrical and optical properties useful as conductive buffer layers for high-temperature YBCO superconductors [42].

We will focus here on a new route to control the texture in ITO films using an original approach that combines the advantages of ion beam sputtering (IBS) and oblique angle deposition (OAD). On the one hand, IBS is a PVD process rarely combined with OAD geometries, which provides high tunability of energies, fluxes and particle species involved during the fabrication [43] and is suitable for low temperature growth of crystalline ITO films with relevant properties (low electrical resistivity $\rho = 1.5 \times 10^{-4}\,\Omega$ cm, visible transmittance >80%) [44,45]. On the other hand, OAD offers an extra degree of freedom for tuning the texture thanks to the adjustment of the incident flux inclination onto the substrate [46]. In previous works, this approach was used for the first time for ITO films and we demonstrated the potential of combining IBS and OAD to manufacture crystalline ITO structures directly at room temperature, with original and adjustable nanostructures and characteristics, including lowered optical indices through the control of the porosity, enhanced optical properties in the near-infrared range and birefringence in the visible range and infrared ranges [47,48]. However, although we evidenced that the combined influence of the sputtering species and the deposition angle can strongly impact the out-of-plane preferred orientation, a better description of the texture development (out- and in-plane) in ITO films prepared by IBS and OAD processes is still needed, which will be the aim of the present study.

2. Material and methods

2.1. Thin film preparation

Crystalline In_2O_3:Sn films were grown at room temperature on (0 0 1) silicon substrates by ion beam sputtering deposition according to Ref. [47]. The deposition chamber is depicted in Fig. 1a. Ar or Xe ion beams of 1.2 keV with a current of 80 mA produced by the primary radio-frequency source was used to sputter a 15 cm diameter water-cooled sintered ceramic target of ITO (90 wt.% In_2O_3, 10 wt.% SnO_2) with an angle of 45° (±3° due to beam divergence). The base pressure in the vacuum chamber was 2×10^{-6} Pa. During the process, the assistance gun was used to introduce a constant oxygen flow of 5 sccm (without energy) in order to achieve films with composition as close as possible to the nominal stoichiometry, and the working pressure was maintained to 2×10^{-2} Pa. Preparation of films at different deposition angles α ranging from 50 to 85° (measured with respect to the substrate normals), by steps of 5°, was achieved in the very same run by positioning the specimen holder of the chamber in the horizontal position (see Fig. 1a) and by placing on it a dedicated laboratory-made OAD holder composed of machined wedges of different inclinations on which substrates pieces are mounted (Fig. 1b). The distance between the center of the target and the center of the OAD holder was 24 cm. According to the deposition time (2 h) and to the total thickness of each films extracted from ellipsometry measurements [47], the deposition rates for Xe and Ar primary ions are about 1.1 Å/s and 0.8 Å/s respectively. More details about the nanostructure and composition of these films are given in Ref. [47].

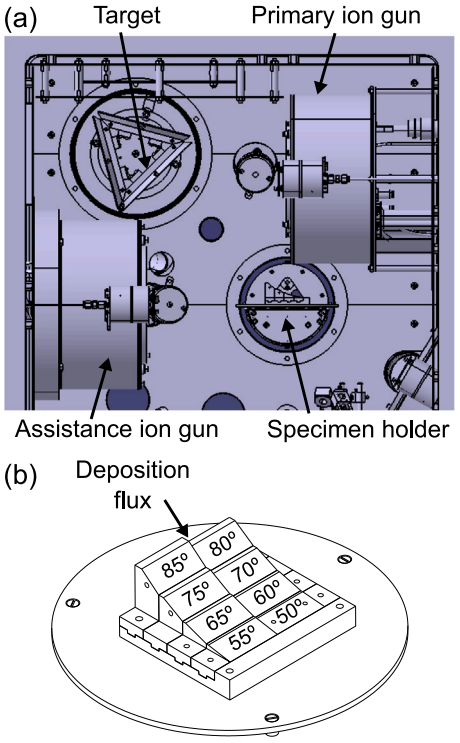

Fig. 1. (a) Cross-section schematics of the IBS deposition chamber showing the guns, the target and the positioning of the substrate holder for OAD configuration. (b) Schematics of the machined OAD substrate holder where the deposition angles α are indicated on each wedge.

2.2. Characterization methods

The crystal structure and orientations of the ITO films was studied by X-ray diffraction (XRD) using a four circle Seifert diffractometer with the K_α wavelength (1.5418 Å) of a copper source. $\theta - 2\theta$ patterns were recorded for 2θ ranging from 20 to 65°, which allows covering the main diffraction lines of the expected cubic bixbyite-type ITO phase (space group Ia-3, No. 206), namely 1 1 2, 2 2 2, 0 0 4, 0 4 4 and 2 2 6, while avoiding the main 0 0 4 peak from the Si substrate at $2\theta \approx 69.2°$. In this Bragg–Brentano geometry, the scattering vector remains perpendicular to the sample surface so that only out-of-plane texture information is accessible. To analyze with more details both the out-of-plane and in-plane texture of the ITO films and its evolution as a function of the deposition angle, XRD pole figures (PFs) measurements were performed. These experiments were carried out for the {2 2 2} and {0 0 4} reflections at several (ϕ, ψ) angles (using constant 2θ Bragg angle for each case), were ϕ represents the azimuthal angle and ψ is the angle between the normal to the sample surface and the normal to a given $(h\,k\,l)$ diffraction plane.

The surface morphology of the deposited films was analyzed by scanning electron microscopy (SEM) in a FEI Teneo microscope fitted with a Schottky field emission gun operated at 2 kV and using secondary electrons for imaging. Transmission electron microscopy (TEM) experiments were also carried out in a JEOL 2010F and in a FEI Talos microscopes operated at 200 kV in order to assess both the local morphology and structure using conventional bright-field (BF) and high-resolution TEM (HRTEM) imaging modes. For that purpose, cross-section lamellae were prepared accordingly to Ref. [49], being first polished and thinned down to less than 10 µm by flat-type tripod polishing and then made electron transparent by a short ion milling step in a GATAN PIPS apparatus (about 30 min at 3.5 keV and ±7° incidence, followed by a final step at 2.5 keV and ±5° during a few minutes).

3. Results and discussion

3.1. Overall out-of-plane orientation evolution

Fig. 2a and Fig. 2b compare the $\theta - 2\theta$ diffractograms of ITO films prepared at different deposition angles using either argon or xenon ions, and clearly show that the sputtering ions have a significant impact on the preferred out-of-plane orientation. Although these data have been published in one of our previous works [47], they are reported here as they appear essential to fully understand the evolution of texture in our films. In the case of Ar, deposition up to angles of $\alpha \approx 80°$ lead to a dominant sharp peak corresponding to the {2 2 2} planes of ITO In_2O_3 cubic-C phase (expected at $2\theta \approx 30.6°$, according to JCPDS 71-2194), which reveals strong out-of-plane preferred ⟨1 1 1⟩ orientations. In these films, a very weak diffraction peak attributed to the 0 4 4 line (expected at $2\theta \approx 51.0°$) can also be detected. For the highest deposition angle, changes are observed since the 2 2 2 line has almost disappeared and a new but still weak peak 0 0 4 reflection starts to grow (expected at $2\theta \approx 35.5°$). Besides the weak and almost constant 0 4 4 peak, similar to the case of Ar deposition, the overall behavior of the Xe films is significantly different. At low deposition angles ($\alpha < 65°$), a sharp 2 2 2 line is dominant whereas the 0 0 4 becomes stronger and predominate for $\alpha > 75°$. As α increases, the 2 2 2 intensity is progressively dropping whereas 0 0 4 is rising, revealing a switching in the out-of-plane texture of the ITO films from (1 1 1) to (0 0 1).

To describe more quantitatively the evolution of the preferred out-of-plane orientation in both ITO films batches, the texture coefficient $TC(hkl)$ was calculated using the following expression [50]:

$$TC(hkl) = \frac{I^{hkl}/I_0^{hkl}}{\frac{1}{N}\sum I^{hkl}/I_0^{hkl}} \quad (1)$$

where I^{hkl} refers to intensities of the $h\,k\,l$ lines extracted from XRD patterns, N is the number of diffraction peaks considered, and I_0^{hkl} is the intensity of reference diffraction pattern (according to JCPDS 71-2194). The higher value of texture coefficient indicates the preferred orientation of the films along specific diffraction plane. The evolution of the texture coefficients versus the deposition angle for the three major reflections detected (2 2 2, 0 0 4 and 0 4 4) is shown in Fig. 2c and d for Ar and Xe deposition, respectively. This confirms the main observations made on the diffractograms: (i) ITO films prepared with Ar are (1 1 1) textured for deposition angles below 85°, while a texture change from (1 1 1) to (0 0 1) initiates for $\alpha = 85°$; (ii) the ITO films prepared with Xe are highly (1 1 1) textured at low deposition angles (<65°) and highly (0 0 1) textured at high deposition angles (>75°); (iii) for α between 60° and 80°, a clear switching process in the preferred orientation is observed; (iv) in both Ar-deposited and Xe-deposited films, a minor (0 1 1) texture is also present and maintained.

3.2. Texture evolution in ITO Xe-deposited films

As proved, the use of Xe during the IBS-OAD deposition process lead to significant changes in the preferred out-of-plane orientation of ITO films with the deposition angle in comparison to the Ar case. To better understand this original texture development, we will focus here on an in-depth analysis through XRD pole figures measurements (Fig. 3) that will be complemented by intensity ψ profiles (Fig. 4) along specific ϕ directions ($\phi = 0°$ in Fig. 4a, $\phi = 45°$ in Fig. 4b). A description of their evolutions in specific deposition angle ranges is given hereafter.

Lowest and intermediate deposition angles

At the lowest deposition angle ($\alpha = 50°$, the {2 2 2} PF presents one sharp central pole as well as intensity reinforcements distributed isotropically at $\psi \approx 70°$ (Fig. 3a) and (Fig. 4a), which reveals an uniaxial (1 1 1) fiber-like texture with preferred [1 1 1] out-of-plane orientation and mostly random in-plane orientations. As α increases up to $\alpha = 70°$, the {2 2 2} intensity on the PFs (Fig. 3b–e) concentrates mainly along $\phi = 0°$ and at specific tilts angles, which suggests the development of a biaxial (1 1 1) texture (with preferential out-of-plane and as in-plane alignments). The single central (2 2 2) pole observed previously for $\alpha = 50°$ has now split into two main off-axis (2 2 2) poles, one shifted towards the incoming flux direction (i.e. at positive ψ tilts) and the other one shifted towards the opposite direction (i.e. at negative ψ tilts). The fact that the (2 2 2) poles are moving away from the PFs center as α increases fully supports the gradual 2 2 2 intensity loss on the $\theta - 2\theta$ diffractograms in Fig. 2b. Intensity profiles of the {2 2 2} PFs recorded along $\phi = 0°$ (Fig. 4a) show two pairs of correlated peaks separated in each set by $\Delta\psi \approx 70°$ (which is a typical angle between {1 1 1} planes in cubic crystals, theoretically 70.5°). They are attributed reflections that could arise from two (1 1 1) variants with different off-axis inclinations (see stereographic projections on Fig. 4d), that vary with α. Multiple Gaussian fitting of these profiles (Fig. 4c) allows extracting the inclination ψ_{111} of each (1 1 1) variant along $\phi = 0°$, from the positions of the main (2 2 2) poles (those closer to $\psi = 0°$). The first (1 1 1) variant (denoted V^1_{111} in the rest of the paper) is inclined towards the deposition flux (with positive tilts), and its inclination increases progressively with α (from $\psi_{111} \approx +5°$ to $\psi_{111} \approx +24°$). The other variant, hereafter V^2_{111}, is initially oriented towards the opposite direction of the deposition flux with negative tilts that are progressively reduced with α (from $\psi_{111} \approx -19°$ to $\psi_{111} \approx -6°$). Meanwhile, no significant intensity reinforcements are noticed along $\phi = \pm 45°$, according to Fig. 4b. Besides tilt considerations, PFs and their intensity profiles along $\phi = 0°$ reveal that the {2 2 2} reflections related to V^1_{111} becomes progressively predominant with α, while those linked to V^2_{111} tends to vanish (see Figs. 3 and 4).

From the measured ψ_{111} tilts for each (1 1 1) variant, the theoretical positions of the others {2 2 2} poles on the PFs were then computed using the WinWULFF module included in the JCrystalSoft software suite. On the PFs and intensity profiles, the expected poles of V^1_{111} and V^2_{111} are displayed respectively as up- and down-pointing triangle symbols. As a convention, variants inclined towards the flux direction are shown in red color, whereas they are shown in green color when tilted towards the opposite direction. From this analysis, we conclude that a dual biaxial texture made of two (1 1 1) off-axis growth variants with specific in-plane rotations is necessary to correctly describe the intensity distribution on the PFs. According to the stereographic projections, those variants can be sketched by tetrahedrons limited by {1 1 1} faces and ⟨1 1 0⟩ edges (Fig. 4d): in the case of V^1_{111}, one edge is oriented towards the incoming particle flux, whereas V^2_{111} corresponds to a 180° in-plane rotation relative to V^1_{111}, with one {1 1 1} plane facing the deposition flux. Both (1 1 1) variants allow reproducing nicely the other intense {2 2 2} reflections observed on the PFs not only along $\phi = 0°$ (Fig. 3b–e), as confirmed by the extracted 222 intensity profiles (Fig. 4a), but also along other ϕ directions where weaker intensity reinforcements appears. The intensity distribution on the experimental

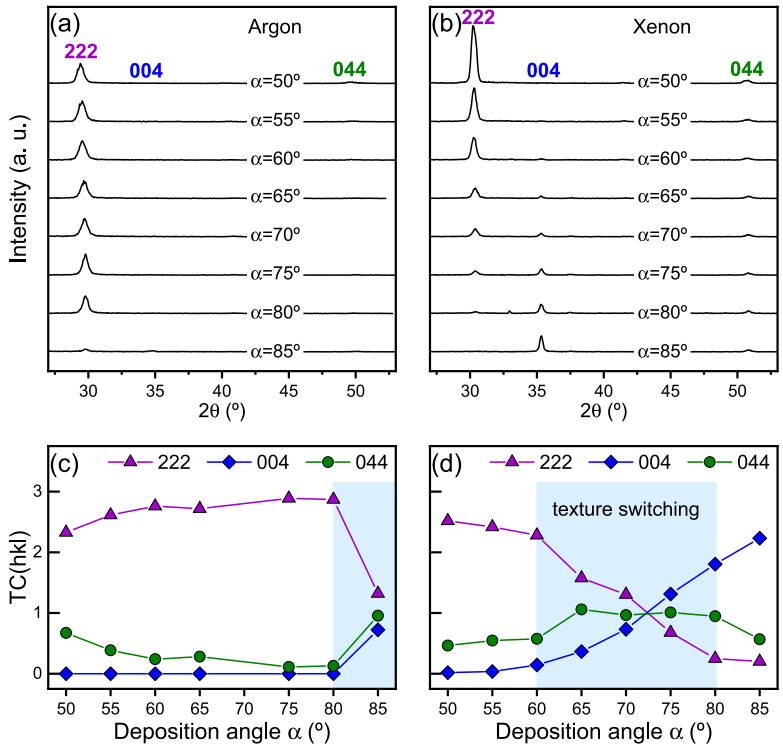

Fig. 2. XRD $\theta - 2\theta$ diffraction patterns recorded at different deposition angles for ITO films prepared by IBS using Ar (a) and Xe (b) ions. The evolution of the texture coefficient versus α obtained from the intensity of the main XRD peaks is shown for Ar (c) and Xe (d) films.

{0 0 4} PF for $\alpha = 70°$ (Fig. 3i) and the very good agreement between the theoretical {0 0 1} poles positions confirm the development of such a dual biaxial off-axis (1 1 1) texture. Moreover, the differences observed in the rocking curves of the main (2 2 2) poles supports this idea of two grain families (for the V^1_{111}, the main (2 2 2) pole is elongated along $\phi = 0°$ whereas it takes place perpendicularly for V^2_{111}).

It is important to highlight that despite similar textures with preferred out-of-plane orientations tilted away from the substrate normal and eventually different growth variants have been reported in pure metals and metal nitrides films prepared by OAD [20,24,26,51], and in co-sputtered OAD Mg-M-O layers, the present results appears quite unusual in such ITO films. A possible origin of such texture evolutions generated during the IBS-OAD process will be discussed later in Section 3.3.

High deposition angles

For greater deposition angles ($\alpha > 70°$), {2 2 2} PFs and extracted intensity profiles are drastically modified (Figs. 3 and 4). On the {2 2 2} PFs, reinforcements located along specific directions $\phi = \pm 45°$ are now clearly visible for tilts around $\psi \approx \pm 54°$ (Figs. 3f–h, 4b). Those poles become sharper and dominant as the deposition angle increases. At the same time, a {0 0 4} pole arises slightly below the center of the PFs and progressively moves towards the PFs center with α (Fig. 3j–l). These features reveal the progressive development of a preferred biaxial (0 0 1) texture (confirmed by the theoretical poles shown in squares symbols on the stereographic projection, Fig. 4d), in line with the preliminary observations made on the $\theta - 2\theta$ diffractograms. Such variant labeled V_{001} is sketched by an octahedron limited by {1 1 1} faces with an ⟨1 1 0⟩ edge towards the incoming flux.

3.3. Possible texture mechanisms

As evidenced, ITO films deposited at room temperature by IBS using Xe ions present an unconventional texture behavior, with different well-defined regimes that depends on the incidence angle of the vapor flux on the substrate. From $\alpha = 50°$ to $\alpha = 85°$, texture changes from a fiber-like (1 1 1) texture to a biaxial (0 0 1) texture, with intermediate biaxial texture states showing preferred off-axis orientations, which turns out to be a specific feature of IBS-OAD process. In the following, the overall crystal orientation information of the films obtained from XRD (Sections 3.1 and 3.2) will be confronted to morphological and structural features evidenced at the nanoscale by SEM and TEM. Projected area calculations of the crystal habits will also be considered to evaluate the ability of different configurations of grain orientations to incorporate incoming particles from the vapor flux by direct capture and establish whether this process is a predominant or not in the development of the crystallographic texture.

Dual biaxial off-axis (1 1 1) texture development

At the lowest deposition angle ($\alpha = 50°$), Xe-deposited films present a [1 1 1] preferred orientation without clear in-plane arrangements. Such (1 1 1) fiber-like texture has been reported previously in ITO thin films deposited by magnetron sputtering under normal incidence and in sufficiently rich oxygen atmosphere [52]. According to Fig. 5a, the film surface looks compact without evidence of porosity. Flat terraces are mostly observed, and no clear morphological surface organization is pointed out, except in some dispersed areas where small lamellar structures usually oriented towards the flux are visible.

Nanoscale inspection by TEM (Fig. 6a) confirms that these lamellar features are isolated, with limited extension (a few hundred nanometers along the depth and in the plane of the film). HRTEM analyses unravel that such ordered surface structures of nanometric dimensions (about 10 nm width) present a preferred [1 1 0] out-of-plane orientation (with a slight tilt of a few degrees towards the flux), which corroborates the presence of the weak 0 4 4 line on the $\theta - 2\theta$ diffractograms (Fig. 2). Fast Fourier transform (FFT) shows that these nanostructures are compatible with off-axis V^2_{111} variant tilted by about 30° in the opposite direction of the flux ($(2\,2\,\bar{2})$ and (2 2 2) planes are tilted by $\psi \approx +40°$ and $\psi \approx -30°$ relative to the substrate surface), in agreement with the weak reinforcements observed on the {2 2 2} PFs along the flux in

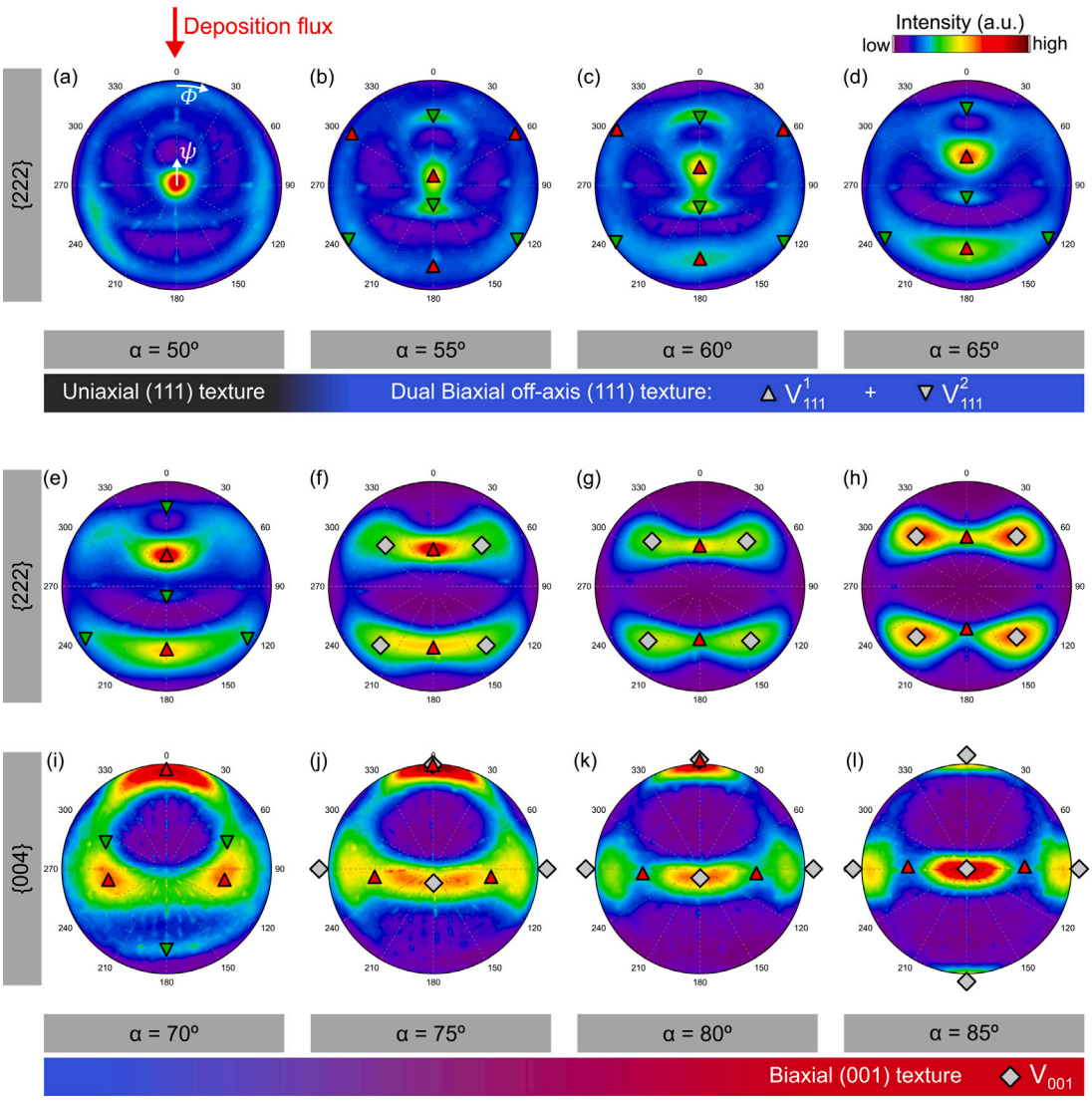

Fig. 3. XRD poles figures of ITO films prepared by IBS with Xe ions at different deposition angles. (a)–(h): {2 2 2} PFs for α ranging from 50 to 85° by steps of 5°. (i)–(l): {0 0 4} PFs for α ranging from 70 to 85° by steps of 5°. Symbols correspond to theoretical poles of different crystallographic variants, according to Fig. 4d. See text for more details.

the opposite direction at such tilt angles. Such isolated nanostructures differs significantly from the rest of the film made of [1 1 1]-oriented larger grains (hundreds of nanometers in size, slightly inclined towards the deposition flux by a few degrees) that match with the position of the main (2 2 2) central pole on the PF (Figs. 3 and 4). These observations could therefore reveal the beginnings of dual biaxial off-axis (1 1 1) texturing.

For $55 \leq \alpha \leq 70°$, the formation of two (1 1 1) variants with specific in-plane orientations, and with off-axis inclinations and relative proportions that vary with α suggests that a competitive growth process may take place. According to SEM and TEM observations, the film surface prepared with $\alpha = 70°$ (Figs. 5b and 6b) now consists in well-separated nanocolumns that are slanted towards the deposition flux. The presence of faceted terminations visible on top-view SEM observations (Fig. 5b) is typical of zone T conditions of the extended structure zone model (SZM) defined by Mahieu et al. [19]. This indicates that the mobility of adatoms is high enough to allow grains to grow according to their kinetically defined crystal habits which are delimited by crystallographic planes that present the lowest normal growth rate (i.e. planes that offer the lowest number of nearest neighbors to incoming adparticles) [19]. In the case of ITO with a bixbyite-type structure, which corresponds to a fluorite-like structure with structural oxygen vacancies, we can reasonably assume that the number of nearest neighbors offered by the growing low-index planes should be the same than for other fluorite-like structure materials like YSZ [53]. Therefore, as for YSZ, {1 1 1} planes of ITO that have the smallest number of nearest neighbors should form facets, leading to columns endings delimited by {1 1 1} surfaces (i.e. {1 1 1} crystal habits) [54]. Note that terminations with tetrahedrons-like shapes and with one edge oriented towards the deposition flux are frequently observed on SEM images and are consistent with the projection of the {1 1 1} planes of the dominant V^1_{111} variant tilted by about 20° towards the flux. Due to enhanced shadowing effect ascribed to OAD, change in the surface roughness and the impingement area offered by the nanocolumns terminations are expected, which may lead to a selective development of grains with specific orientations due to difference in their growth rates, as reported previously for other materials like MgO and Cr [28,55,56]. According to previous studies reported on other systems [19,51,57], the original texture development reported here for ITO might be driven by the capture of incoming particles by growing crystal habits.

To verify this idea and evaluate the most favorable configurations for catching incident particles, the direct capture area σ of ITO grains with [1 1 1] out-of-plane orientation and {1 1 1} crystal habits (represented by tetrahedrons limited by {1 1 1} faces) has been calculated as

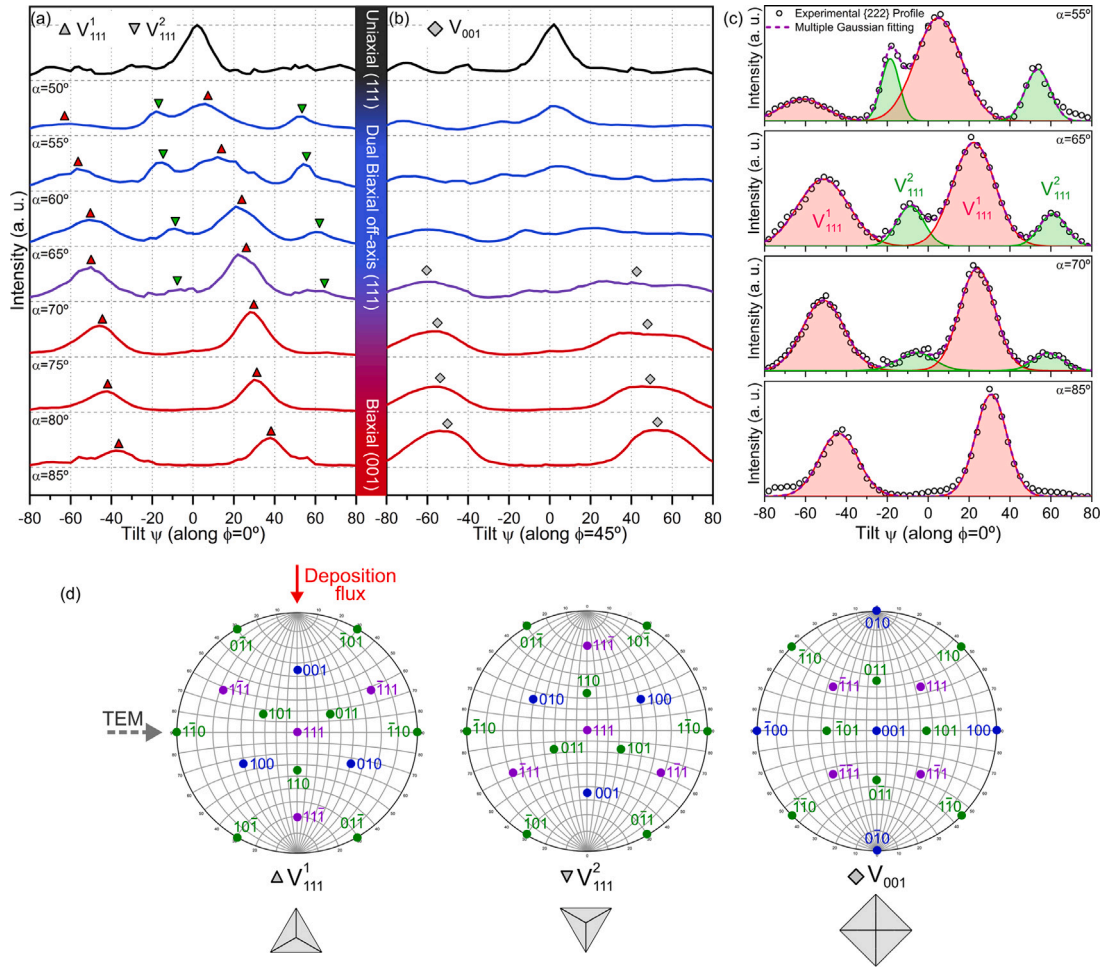

Fig. 4. ψ intensity profiles of {2 2 2} PFs shown in Fig. 3 recorded for different deposition angles along specific ϕ directions: (a) $\phi = 0°$ and (b) $\phi = 45°$. Up-pointing and down-pointing triangles refer to both (1 1 1) variants, according to Fig. 4d. Color scheme was used to indicate in which direction are tilted those variants (red: towards the incoming flux, green: opposite to the incoming flux). Squares refer to the (0 0 1) variant. (c) Fitting of some of the {2 2 2} profiles along $\phi = 0°$. (d) Stereographic projections showing the {1 1 1}, {0 0 1} and {0 1 1} poles of the different variants identified on the PFs (for perfectly oriented grains, without tilt): V^1_{111}, V^2_{111} and V_{001}. The red arrow indicates the direction of the projected incoming deposition flux. The dashed-gray arrow corresponds to the direction for TEM observations. Top-view projection of {1 1 1} planes in each variant are shown at the bottom. More details are given in the text.

a function of the in-plane rotation γ of the crystal habit and the inclination of the deposition flux η relative to the normal of the (1 1 1) base plane, following a methodology similar to that proposed in Ref. [56] (see Fig. 7a and Supporting Information for the calculation details). Although at first glance counter-intuitive if one considers only the number of nearest neighbors offered by the crystallographic planes as the main parameter for the development of the preferred orientation and facets [19], the growth of a cubic crystal along [1 1 1] with {1 1 1} tetrahedral crystal habit is supported by another work on YSZ films with fluorite structure [54]. This might be explained by an anisotropy in the growth rates of the different {1 1 1} planes due to disparities in the momentum transfer of incoming particles depending on the inclinations of the {1 1 1} surfaces [58]. Indeed, when the adparticles arrives on highly tilted planes, the parallel component of their momentum will be higher than in the case of planes with lower tilts, which will contribute to enhance the adatoms lateral diffusion and promote the formation of facets.

Note that the angle η was introduced here to account for eventual off-axis tilt of the variants either towards or in the opposite direction of the particle flux, in addition to the conventional deposition angle α (see inset in Fig. 7b). The σ function evaluation reported in Fig. 7a and b provides useful information. Indeed, it points out two maxima that suggests that two {1 1 1} habits configurations with specific in-plane orientations are more prone to develop, in good agreement with XRD results. The first configuration that corresponds to a {1 1 1} crystal habit with a ⟨1 1 0⟩ edge facing the incoming particle flux (in-plane rotation $\gamma = 30°$, equivalent to V^1_{111}) exhibits a maximal capture area at an incoming flux inclination of $\eta \approx 55°$. The second one, that matches the {1 1 1} crystal habit with one {1 1 1} facet oriented towards the incident flux ($\gamma = 90°$, equivalent to V^2_{111}), presents a maximal capture section for $\eta \approx 125°$. In addition, other local maxima are observed for both configurations at $\eta \approx 110°$ (for $\gamma = 30°$) and $\eta \approx 70°$ (for $\gamma = 90°$).

To go further and better apprehend those calculations, it is relevant to monitor the progress of the incidence angle of the incoming flux on each (1 1 1) variant as a function of the deposition angle (Fig. 7b), using the following expression:

$$\eta(\alpha) = \alpha - \psi_{hkl}(\alpha) \tag{2}$$

where $\psi_{hkl}(\alpha)$ represents the inclination of each $(h\,k\,l)$ variants relative to the surface normal. It is taken positive when the basal $(h\,k\,l)$ planes are tilted towards the deposition flux and negative in the opposite direction (see inset in Fig. 7b). In the present case of (1 1 1) variants, $\psi_{111}(\alpha)$ was extracted from the position of the main (2 2 2) poles obtained after fitting (see Fig. 4). Those plots unravel that the incidence angle of the particles flux on both (1 1 1) variant remains almost constant, $\eta \approx 43 - 50°$ for V^1_{111} and $\eta \approx 73 - 76°$ for V^2_{111} (see full line plots).

Direct capture supports nicely the experiments for various reasons. It not only explains why two different (1 1 1) configurations can be

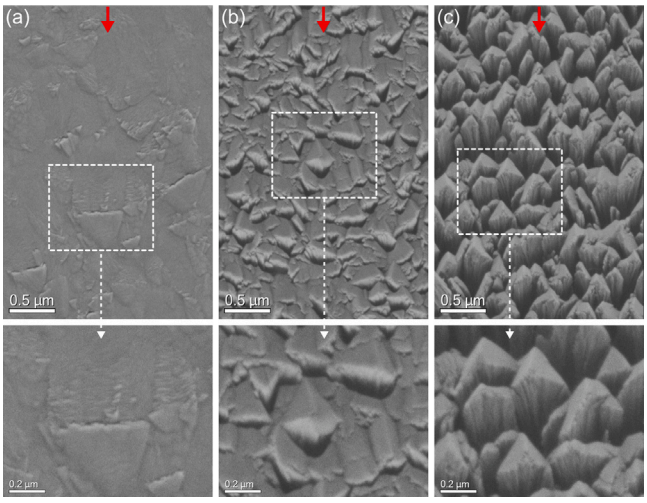

Fig. 5. Top-view SEM images of the Xe films deposited at (a) $\alpha = 50°$, (b) $\alpha = 70°$ and (c) $\alpha = 85°$. The red arrow on top of each SEM micrograph indicates the projection of the incoming particle flux. Magnified regions characteristic of each sample are shown at the bottom.

developed (presence of different maxima for σ in two specific in-plane orientations), but also helps us to interpret the changes in the tilts and intensities observed experimentally on Figs. 3 and 4 for both variants. Indeed, the off-axis [1 1 1] orientations (towards or opposite to the flux), turns out to be driven by the capture area maximization onto the {1 1 1} crystal habits to maintain the effective incidence angle η close to optimal values. The comparison of σ function (Fig. 7a) and $\eta(\alpha)$ evolution (Fig. 7b) indicates that habits corresponding to V^1_{111} are tilted so that the capture is maintained close to its maximum value at $\eta \approx 55°$, while those corresponding to V^2_{111} are tilted according to the local maximum at $\eta \approx 70°$. Hence, (1 1 1) grains with a ⟨1 1 0⟩ edge facing the flux are expected to catch more adatoms by direct capture and therefore to grow preferentially, in good agreement with the trends of V^1_{111} to become progressively dominant for α values ranging from 55° to 70°. This preferential growth is supported by the top-view SEM images for films deposited at $\alpha = 70°$ (Fig. 5b), where faceted tetrahedral shapes with an edge oriented towards the deposition flux are frequently observed at the termination of the nanocolumns, whereas structures with an edge turned in the opposite direction are rarely perceived.

HRTEM micrographs and their FFTs obtained in different areas of the film deposited at $\alpha = 70°$ (Fig. 6b) reveal that the crystal orientation is maintained across individual slanted rods, with the $[1\,1\,\bar{1}]$ direction tilted towards the opposite direction of the incoming flux by $\psi \approx -47°$ relative to the substrate normal. This nicely support our XRD results, accounting for the strong pole observed at $\psi \approx -50°$ on the {2 2 2} PF (Figs. 3e and 4), which is consistent with the $(2\,2\,\bar{2})$ planes of V^1_{111} assuming that this variant is tilted by about 20° towards the flux (see the stereographic projection). It is important to note here that the spot related to (2 2 2) planes of V^1_{111}, which is expected towards the flux at $\psi \approx +20°$ is missing on the FFTs. This is explained by the fact that the $[\bar{5}\,7\,2]$ observation axis actually differs from the expected $[\bar{1}\,1\,0]$ zone axis, with a relative tilt of about 16° that reveals a rotation of the variant which is consistent with the broad {2 2 2} pole on the PF (Fig. 3e). Such rotation remains compatible with direct capture as the global maximum for σ at $(\eta = 55°, \gamma = 30°)$ is large and can cover a wide range of in-plane rotations and out-of-plane tilts. In the thinner dense region near the substrate (≈ 100 nm thick), the [1 1 1] direction is well aligned perpendicular to the surface and corresponds to V^2_{111} without tilt that is assumed to be present but in a much smaller amount in good agreement with PFs. As for the previous case, the observation axis $[5\,\bar{6}\,1]$, that differs from the expected $[1\,\bar{1}\,0]$ zone axis (with a relative tilt of about 9°), indicates slight in-plane rotation of V^2_{111}, which remains compatible with direct capture (large and almost flat local maximum at $(\eta = 70°, \gamma = 90°)$.

(0 0 1) texture development

A deposition angle around $\alpha = 70°$ appears to be crucial for the (1 1 1) to (0 0 1) texture switching. The first symptoms observed for $\alpha \approx 65 - 70°$ consist in an intensity drop of the {2 2 2} reflections primarily attributed to V^2_{111} (Figs. 3 and 4), and in a slight splitting of the {2 2 2} poles initially linked to V^2_{111} is observed, as pointed out by the development of an asymmetry on the {2 2 2} peaks in Fig. 4a. These features could reveal a transitory regime in which some grains in the V^2_{111} configuration, instead of disappearing as supposed up to now, could persist with a tilting of their (1 1 1) basal plane in the direction opposite to the deposition flux (near $\psi_{111} = -51°$ and $\psi_{111} = -47°$ for $\alpha = 65°$ and $\alpha = 70°$, see green dashed line plot in the inset in Fig. 7b) so that (1 1 1) and $(1\,1\,\bar{1})$ planes of V^2_{111} become parallel to the $(1\,1\,\bar{1})$ and (1 1 1) planes of V^1_{111}, respectively. According to σ calculation for the [1 1 1] orientation (Fig. 7a and c), such V^2_{111} tilt could be correlated to an accommodation process aimed at maximizing the incorporation of adatoms on {1 1 1} habits through direct capture by maintaining the effective incidence angle near the global maximum at $\eta \approx 125°$. This new configuration for V^2_{111} actually requires sufficiently high deposition angles ($\alpha \approx 65 - 70°$) to reach maximum capture area without tilting too much the habit, which is not the case for V^1_{111} whose capture maximization actually requires moderate tilts.

For $\alpha \approx 70°$, only one pair of {2 2 2} reflections remains visible along $\phi = 0°$ (Fig. 4). Following the previous idea, both (1 1 1) variants, tilted either towards (V^1_{111}) or opposite (V^2_{111}) to the deposition flux, should be maintained for $\alpha > 70°$, with inclinations η that allows a maximization of the capture section by the {1 1 1} habits with [111] orientations. Note however that these {2 2 2} contributions related to dual biaxial off-axis (1 1 1) texture progressively vanishes as α increases. At the same time, the (0 0 1) texture progressively develops, according to the {2 2 2} intensity reinforcements observed on the PFs at $\psi \approx \pm 54°$ along $\phi = \pm 45°$, and to the appearance of the (0 0 4) pole near the PFs center (Fig. 3(j)–(l)). This (0 0 4) pole, initially tilted by $\psi_{001} \approx -11°$ for $\alpha = 75°$, progressively moves towards the center with α (see inset in Fig. 7b). Intensity reinforcements along specific directions ($\phi = 0°$, $\phi = \pm 90°$) at ψ tilts near ±90° from the PF center confirm the progressive development of the (0 0 1) biaxial texture with the [0 0 1] axis becoming almost perpendicular to the surface.

To better describe the origin of such texture, calculations of the capture area of incident particles in the case of [0 0 1] out-of-plane orientation were carried out using a similar approach than for the [1 1 1] case (see Supporting Information). For that, assuming that {1 1 1} crystal habits are maintained, [0 0 1]-oriented grains can be represented by octahedrons with {1 1 1} triangular facets. According to Fig. 7c and Fig. 7e, $\sigma(\eta, \gamma)$ presents a maximum for $\eta = 90°$ and an in-plane rotation of $\gamma = 45°$. This configuration corresponding to the V_{001} variant (Fig. 4d) is in line with the XRD results and is also fully supported by SEM observation the film deposited at $\alpha = 85°$ (Fig. 5c). The micrograph shows substantial modification of the surface morphology as compared to the film prepared at $\alpha = 70°$, with nanocolumns that appear more separated and more tilted towards the deposition flux, most of them with faceted terminations that consist in truncated octahedrons with one edge oriented towards the deposition flux. Note that the regions facing the flux look flat whereas the shadowed parts of the columns present a fibrous aspect. HRTEM analyses done in the upper region of the film across an isolated column allows explaining these two regions in terms of different crystallinity (Fig. 6c): the region facing the deposition flux has a monocrystalline character which corresponds to the area with large facets on the SEM image, whereas the truncated rear region of the column present a nanocrystalline character with aligned nanometric sub-columns tilted by about 45° towards the flux. According to FFTs, the same crystal orientation is maintained in both regions. In the present case, (1 0 3) planes are found almost parallel to the surface.

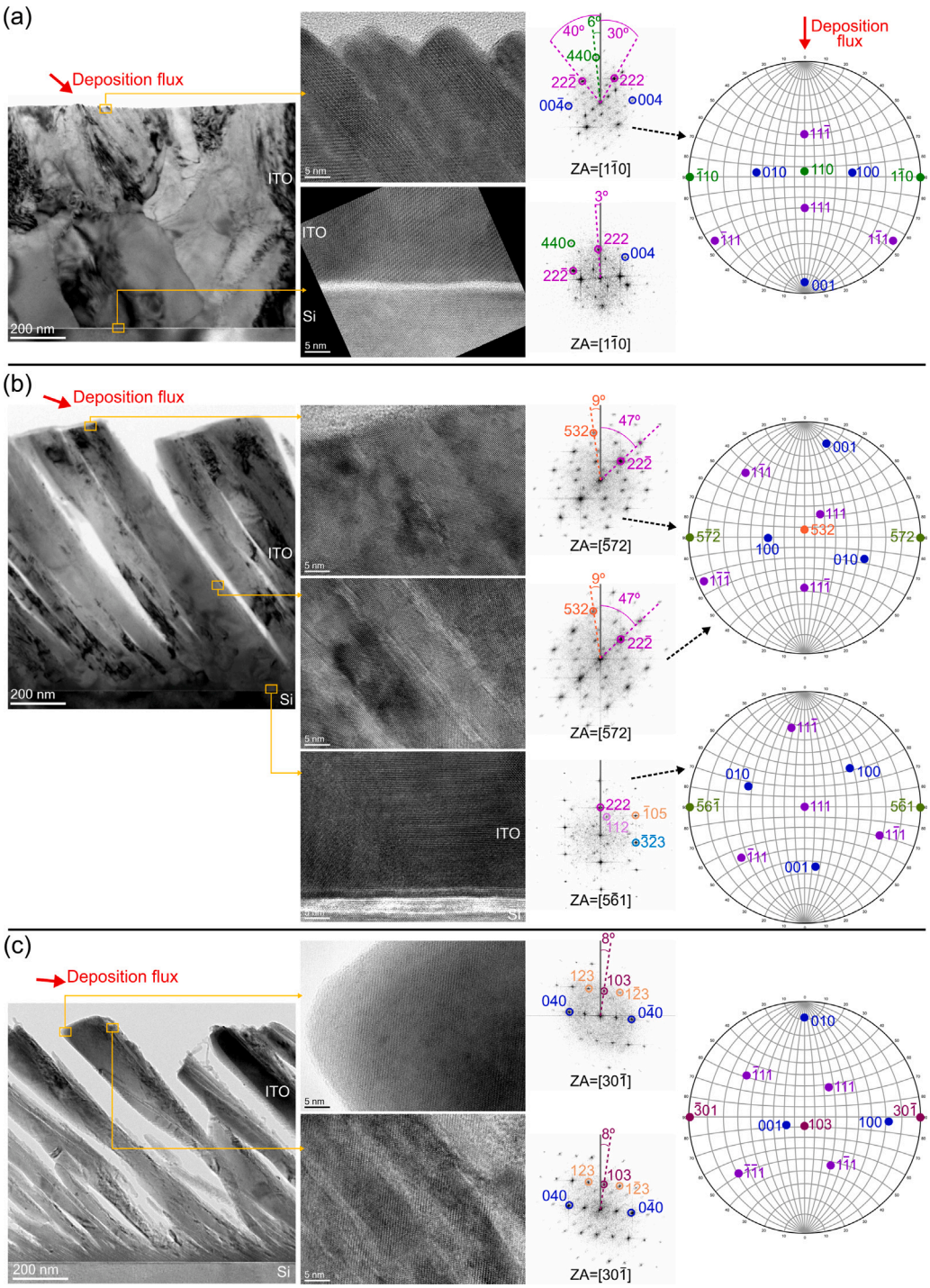

Fig. 6. BF-TEM and HRTEM observations of the ITO films deposited with Xe at different angles. (a) $\alpha = 50°$, (b) $\alpha = 70°$ and (c) $\alpha = 85°$. On the right are shown typical indexed FFT, and the corresponding stereographic projection deduced from FFTs. The normal to Si-(0 0 1) planes of the substrate was used as a reference for angle determination.

According to stereographic projections, the identified [3 0 $\bar{1}$] observation axis that differs from the expected [1 0 0] zone axis (relative tilt of about 18°) is consistent with the V_{001} variant that would be rotated and tilted, in agreement with the broad {0 0 4} pole on the PFs. As for the [1 1 1] case, the ψ_{001} tilts of the main (0 0 4) pole (obtained by fitting the {0 0 4} intensity profiles along $\phi = 0°$, not shown here) have been used to plot the evolution of the incidence angle $\eta(\alpha)$ of the particle flux on the crystal habits (using Eq. (2)), which remains constant near $\eta \approx 90°$, revealing that this specific biaxial (0 0 1) texture is also driven by the direct capture maximization of adatoms on the {1 1 1} habits.

As Xe deposition conditions are ascribed to zone T of the SZM in which grains with the geometrically fastest growing direction perpendicular to the substrate overgrows the other grains (evolutionary selection), the change in the preferred out-of-plane orientation from [1 1 1] to [0 0 1] with α indicates a modification in the perpendicular growth rates of the (1 1 1) and (0 0 1) planes parallel to the surface. Despite hypothetical, the origin of this α-dependence could be found in an evolution of adatoms surface diffusion promoted by changes in the normal and tangential components of the momentum transfer on the crystal planes.

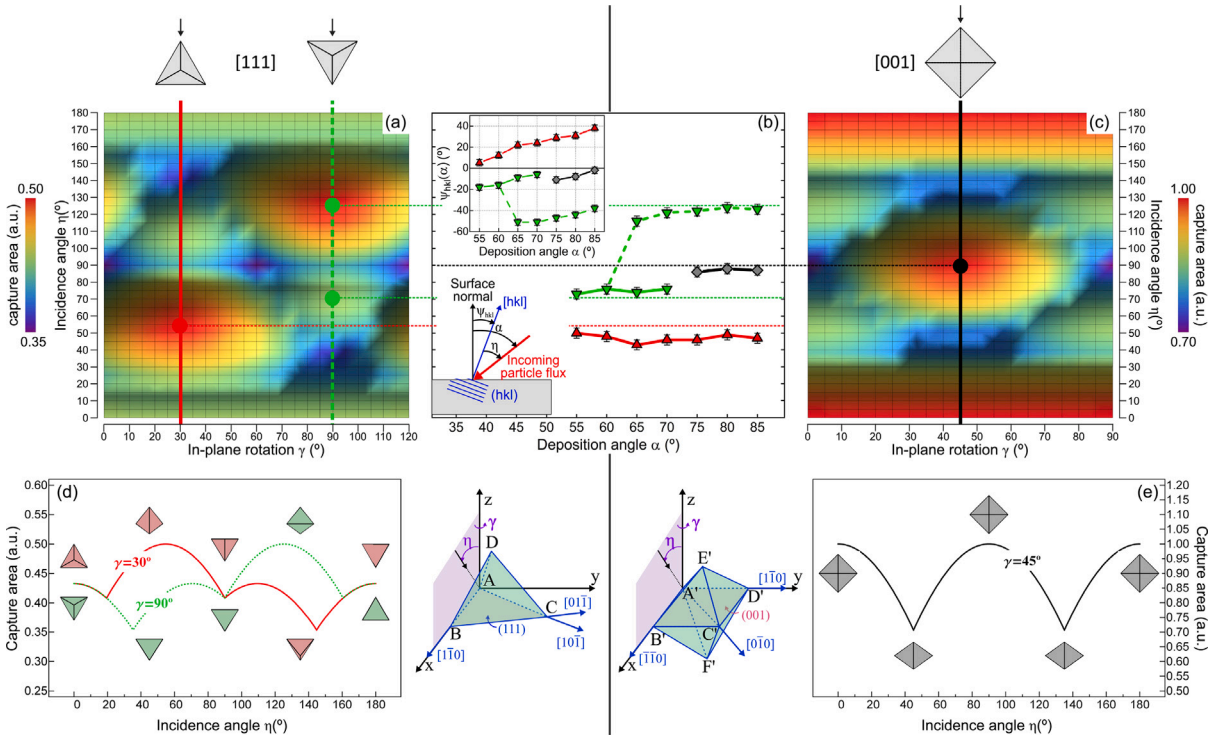

Fig. 7. Calculated direct capture areas $\sigma(\eta,\gamma)$ for {1 1 1} crystal habits with (a) [1 1 1] and (c) [0 0 1] out-of-plane orientations, as a function of the inclination angle η (that can be greater than 90° due to crystal habit tilting) and the in-plane rotation γ (see Supporting Information for more details). On top are shown top-view schematics of {1 1 1} crystal habits for specific in-plane rotations of interest relative to the deposition flux indicated by arrows ($\gamma = 30°$ and $\gamma = 90°$ for [1 1 1], $\gamma = 45°$ for [0 0 1], respectively). (d) and (e) show the $\sigma(\eta)$ profiles for the specific in-plane orientation evidenced on (a) and (c) (discontinuities occur when {1 1 1} planes are hidden by other planes). Insets in (d) and (e) shows some projections of the crystal habits as "seen" by the incoming particles. In between are depicted the geometries used for calculations. (b) Evolution of the incidence angle $\eta(\alpha)$ of the deposition flux on each $(h\,k\,l)$ variant identified on the PFs. Insets explains the different angles and show the $\psi_{hkl}(\alpha)$ tilts extracted from the PFs. The horizontal dotted line reports the η values that maximize $\sigma(\eta,\gamma)$ according to calculations.

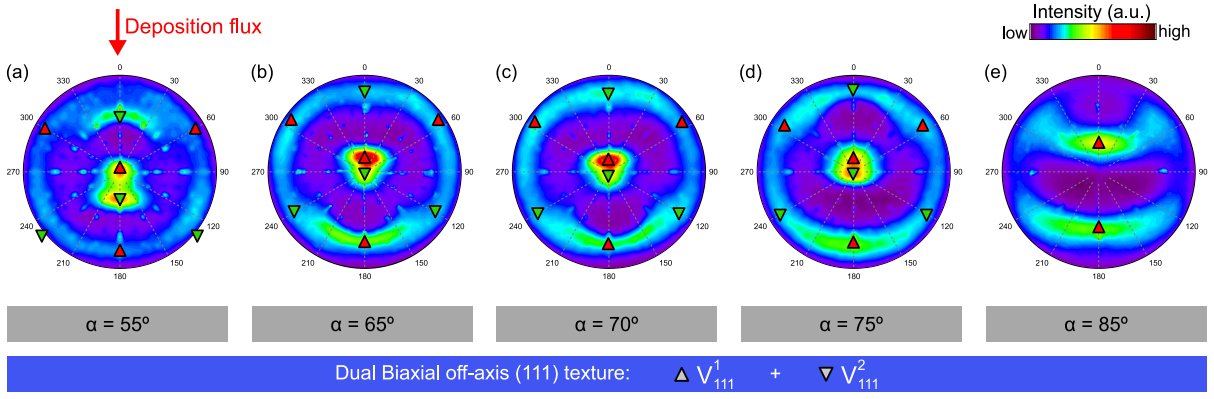

Fig. 8. {2 2 2} XRD poles figures of ITO films prepared by IBS with Ar ions at different deposition angles: (a) $\alpha = 55°$, (b) $\alpha = 65°$, (c) $\alpha = 70°$, (d) $\alpha = 75°$, (e) $\alpha = 85°$. Symbols correspond to theoretical poles of different crystallographic variants, according to Fig. 4d. See text for more details.

To further elucidate the possible mechanisms that could drive the texture in ITO films prepared by IBS-OAD, it is insightful to compare its evolution depending on the type of ions used to sputter the target that appears as a key factor. Indeed, as reported in Section 3.1, significant differences are observed when Ar ions are used as sputtering ions instead of Xe, with the development of [1 1 1] out-of-plane preferred orientation whatever the deposition angle is, but without (1 1 1) to (0 0 1) transition. Deeper analysis through PFs (Fig. 8) reveals that the (1 1 1) texture of Ar-deposited films consists in a dual biaxial off-axis [1 1 1] out-of-plane preferred orientation apparently similar to that of Xe-deposited films. Nevertheless, tilts of both V^1_{111} and V^2_{111} variants appear more limited and do not vary monotonously with α (contrary to Xe, see inset in Fig. 7b), which suggests that Ar growth is not dominated by a direct capture process. Note that for $\alpha = 85°$ (Fig. 8e) the {2 2 2} planes start to tilt far away but without evidence of {0 0 1} texture which supports the full intensity loss observed for 2 2 2 reflection and the absence of 0 0 4 line on the XRD diffractogram (Fig. 2). These differences between Ar- and Xe-deposited films may be explained by the energies involved during the IBS process which depends strongly on the mass ratio of the interacting particles [43]. According to Monte-Carlo SRIM calculations performed in our previous work, Ar sputtering leads to substantially more energetic conditions (for backscattered ions and to a lesser extent for the sputtered atoms) than Xe sputtering (for the same primary energy) [47], which results in a higher surface mobility [43]. Adatoms in the Ar sputtering process are therefore expected to be more active to promote a restructuring of grain growth according to {1 1 1} planes of lower surface tension [59] parallel to the substrate in line with the zone II growth model [19], hence hindering

the direct capture process. On the contrary, the use of Xe as sputtering ions fulfills sufficiently low mobility deposition conditions (due to the lower adatoms energy) to promote orientation retention following the zone T growth model [19]. Such differences in the adatoms mobilities is supported by observations made in our previous study showing that for the very same deposition conditions, Ar-deposited films appear noticeably denser and exhibit flatter top surfaces (instead of faceted habits in the case of Xe deposition) [47]. This idea also agrees with some works on metal films (Cr, Fe) prepared by OAD using different deposition processes which attribute the texture switching from a more to less energetically favorable preferred orientation to a combined effect of self-shadowing and surface diffusion of adatoms [60,61].

4. Conclusion

This work reports a comprehensive study devoted to assess the texture in In_2O_3:Sn films prepared at oblique incidence by ion beam sputtering, with particular emphasis on the influence of the vapor incidence α on Si substrates (from 50° to 85°) and on the sputtering ions (argon or xenon accelerated at 1.2 keV). XRD, SEM, and TEM experiments have been used to unravel possible key mechanisms involved in its development. When Xe is used to sputter the target during the IBS process, an original evolution depending on the deposition angle α is evidenced. (i) For $\alpha \leq 70°$, a dual biaxial off-axis [1 1 1] out-of-plane preferred orientation takes place, which mostly consists in two (1 1 1) variants with specific in-plane orientation and different off-axis inclinations that change monotonously with α. (ii) For intermediate deposition angles around $\alpha \approx 70°$, a switching from [1 1 1] to [0 0 1] occurs, the films becoming biaxially (0 0 1)-textured with a defined in-plane orientation at the highest deposition angles. These different behaviors are well described by a direct capture maximization of adatoms on the {1 1 1} habits of the ITO cubic bixbyite phase, shedding lights on the out-of-plane tilts and in-plane rotations evidenced of the different crystal variants. Such process is however made possible only when adatoms mobility is high enough but also sufficiently low to allow grains to grow according to their kinetically determined crystal habits, which is not the case when Ar is used instead of Xe during IBS deposition. In that case, diffusivity of adparticles might be exalted, making growth conditions driven by surface energy concepts rather than direct capture mechanism. For this reason, only preferred out-of-plane orientation driven by thermodynamical concepts according to (1 1 1) planes of lower surface tension parallel to the surface is observed.

Besides the new insights on fundamental aspects of thin films deposition processes, this work demonstrates that IBS-OAD is a powerful and attractive route for the nanoengineering of porous and nanostructured ITO surfaces with tailored crystal orientations (both out-of-plane and in-plane) in particular for applications requiring low temperature processing and for which crystal orientations can be a key factor. Finding direct correlations between texture and properties in such OAD films is however not straightforward and would require dedicated studies because other morphological features (including porosity, column size and tilt, surface roughness) with possibly strong impact may also be modified when deposition parameters are changed.

CRediT authorship contribution statement

Bertrand Lacroix: Conceptualization, Methodology, Software, Writing – original draft, Investigation, Visualization, Funding acquisition. **Fabien Paumier:** Conceptualization, Methodology, Investigation, Resources, Validation, Writing – review & editing. **Antonio J. Santos:** Investigation, Writing – review & editing. **Florian Maudet:** Investigation, Resources. **Thierry Girardeau:** Investigation, Resources. **Cyril Dupeyrat:** Resources. **Rafael García:** Supervision. **Francisco M. Morales:** Supervision, Writing – review & editing.

Declaration of competing interest

The authors declare that they have no known competing financial interests or personal relationships that could have appeared to influence the work reported in this paper.

Data availability

Data will be made available on request.

Acknowledgments

This work has been partly supported by the French "Nouvelle Aquitaine" Region and partly carried out in the framework of the associate laboratory PRIMEO ("Partnership for Research and Innovation in Emerging Materials for phOtonics") between Safran Electronics & Defense and PPRIME Institute. The "Talent Attraction Program" of the University of Cádiz (for supporting BL contracts E-11-2017-0117214 and E-11-2019-0133241), the IMEYMAT Institute as well as the Ministerio de Ciencia, Innovación *y* Universidades and Ministerio de Educación *y* Formación Profesional in Spain (for AJS financial support and grants ICARO-173873 and FPU16-04386) are also acknowledged.

Appendix A. Supplementary data

Supplementary material related to this article can be found online at https://doi.org/10.1016/j.apsusc.2022.154677.

References

[1] C.V. Thompson, R. Carel, Texture development in polycrystalline thin films, Mater. Sci. Eng. B: Solid-State Mater. Adv. Technol. 32 (1995) 211–219, http://dx.doi.org/10.1016/0921-5107(95)03011-5.
[2] D.B. Knorr, J.A. Szpunar, Applications of texture in thin films, JOM 46 (1994) 42–48, http://dx.doi.org/10.1007/bf03222582.
[3] D.B. Knorr, Development of texture in interconnect thin film stacks, J. Vac. Sci. Technol. B 16 (1998) 2734, http://dx.doi.org/10.1116/1.590265.
[4] B.D. Schutter, K.D. Keyser, C. Lavoie, C. Detavernier, Texture in thin film silicides and germanides: A review, Appl. Phys. Rev. 3 (2016) 031302, http://dx.doi.org/10.1063/1.4960122.
[5] A.E. Giba, P. Pigeat, S. Bruyère, T. Easwarakhanthan, F. Mücklich, D. Horwat, Controlling refractive index in AlN films by texture and crystallinity manipulation, Thin Solid Films 636 (2017) 537–545, http://dx.doi.org/10.1016/j.tsf.2017.06.057.
[6] Y. Wang, J. Ghanbaja, P. Boulet, D. Horwat, J.F. Pierson, Growth, interfacial microstructure and optical properties of NiO thin films with various types of texture, Acta Mater. 164 (2019) 648–653, http://dx.doi.org/10.1016/j.actamat.2018.11.018.
[7] C.V. Falub, A. Karimi, M. Ante, W. Kalss, Interdependence between stress and texture in arc evaporated Ti-Al-N thin films, Surf. Coat. Technol. 201 (2007) 5891–5898, http://dx.doi.org/10.1016/j.surfcoat.2006.10.046.
[8] D. Schläfer, K. Fischer, M. Schubert, B. Schlobach, Texture investigations on high temperature superconductors, Texture Stress Microstruct. 24 (1995) 93–103, http://dx.doi.org/10.1155/tsm.24.93.
[9] D.T. Verebelyi, D.K. Christen, R. Feenstra, C. Cantoni, A. Goyal, D.F. Lee, M. Paranthaman, P.N. Arendt, R.F. DePaula, J.R. Groves, C. Prouteau, Low angle grain boundary transport in $YBa_2Cu_3O_{7-\delta}$ coated conductors, Appl. Phys. Lett. 76 (2000) 1755–1757, http://dx.doi.org/10.1063/1.126157.
[10] H.S. Cornejo, L.D.L.S. Valladares, C.H.W. Barnes, N.O. Moreno, A.B. Domínguez, Texture and magnetic anisotropy of $YBa_2Cu_3O_{7-x}$ film on MgO substrate, J. Mater. Sci. Mater. Electron. 31 (2020) 21108–21117, http://dx.doi.org/10.1007/s10854-020-04623-w.
[11] G. Korotcenkov, M. DiBattista, J. Schwank, V. Brinzari, Structural characterization of SnO_2 gas sensing films deposited by spray pyrolysis, Mater. Sci. Eng. B: Solid-State Mater. Adv. Technol. 77 (2000) 33–39, http://dx.doi.org/10.1016/s0921-5107(00)00455-4.
[12] S. Pati, Highly textured ZnO thin films grown using sol-gel route for gas sensing application, J. Alloys Compd. 695 (2017) 3552–3558, http://dx.doi.org/10.1016/j.jallcom.2016.11.414.
[13] B. Pecquenard, F.L. Cras, D. Poinot, O. Sicardy, J.-P. Manaud, Thorough characterization of sputtered CuO thin films used as conversion material electrodes for lithium batteries, ACS Appl. Mater. Interfaces 6 (2014) 3413–3420, http://dx.doi.org/10.1021/am4055386.

[14] L. Hultman, J.-E. Sundgren, J.E. Greene, D.B. Bergstrom, I. Petrov, High-flux low-energy (=20 eV) N^+_2 ion irradiation during TiN deposition by reactive magnetron sputtering: Effects on microstructure and preferred orientation, J. Appl. Phys. 78 (1995) 5395–5403, http://dx.doi.org/10.1063/1.359720.

[15] H. Ji, G.S. Was, J.W. Jones, N.R. Moody, Effect of ion bombardment on in-plane texture, surface morphology, and microstructure of vapor deposited Nb thin films, J. Appl. Phys. 81 (1997) 6754–6761, http://dx.doi.org/10.1063/1.365217.

[16] G.S. Was, H. Ji, Z. Ma, Texture control in thin films using ion bombardment, Texture Stress Microstruct. 34 (2000) 105–118, http://dx.doi.org/10.1155/tsm.34.105.

[17] M. Clement, E. Iborra, J. Sangrador, A. Sanz-Hervás, L. Vergara, M. Aguilar, Influence of sputtering mechanisms on the preferred orientation of aluminum nitride thin films, J. Appl. Phys. 94 (2003) 1495–1500, http://dx.doi.org/10.1063/1.1587267.

[18] S. Suwas, R.K. Ray, Crystallographic Texture of Materials, Springer, London, 2014, http://dx.doi.org/10.1007/978-1-4471-6314-5.

[19] S. Mahieu, P. Ghekiere, D. Depla, R.D. Gryse, Biaxial alignment in sputter deposited thin films, Thin Solid Films 515 (2006) 1229–1249, http://dx.doi.org/10.1016/j.tsf.2006.06.027.

[20] P. Morrow, F. Tang, T. Karabacak, P.-I. Wang, D.-X. Ye, G.-C. Wang, T.-M. Lu, Texture of Ru columns grown by oblique angle sputter deposition, J. Vac. Sci. Technol. A 24 (2006) 235–245, http://dx.doi.org/10.1116/1.2165661.

[21] F. Tang, G.-C. Wang, T.-M. Lu, In situ reflection high energy electron diffraction surface pole figure study of biaxial texture evolution in anisotropic Mg nanoblades during shadowing growth, J. Appl. Phys. 102 (2007) 014306, http://dx.doi.org/10.1063/1.2752131.

[22] L. Chen, T.-M. Lu, G.-C. Wang, Incident flux angle induced crystal texture transformation in nanostructured molybdenum films, J. Appl. Phys. 112 (2012) 024303, http://dx.doi.org/10.1063/1.4737403.

[23] L. Chen, T.-M. Lu, G.-C. Wang, Creation of biaxial body center cubic tungsten nanorods under dynamic shadowing effect, Thin Solid Films 539 (2013) 65–69, http://dx.doi.org/10.1016/j.tsf.2013.04.151.

[24] S. Liedtke-Grüner, C. Grüner, A. Lotnyk, J.W. Gerlach, B. Rauschenbach, Biaxially textured titanium thin films by oblique angle deposition: conditions and growth mechanisms, Phys. Status Solidi A 217 (2020) 1900636, http://dx.doi.org/10.1002/pssa.201900636.

[25] A.R. Shetty, A. Karimi, Texture mechanisms and microstructure of biaxial thin films grown by oblique angle deposition, Phys. Status Solidi b 249 (2012) 1531–1540, http://dx.doi.org/10.1002/pssb.201248010.

[26] R. Mareus, C. Mastail, F. Anğay, N. Brunetière, G. Abadias, Study of columnar growth, texture development and wettability of reactively sputter-deposited TiN, ZrN and HfN thin films at glancing angle incidence, Surf. Coat. Technol. 399 (2020) 126130, http://dx.doi.org/10.1016/j.surfcoat.2020.126130.

[27] M. Bauer, R. Semerad, H. Kinder, YBCO films on metal substrates with biaxially aligned MgO buffer layers, IEEE Trans. Appl. Supercond. 9 (1999) 1502–1505, http://dx.doi.org/10.1109/77.784678.

[28] P. Ghekiere, S. Mahieu, G.D. Winter, R.D. Gryse, D. Depla, Scanning electron microscopy study of the growth mechanism of biaxially aligned magnesium oxide layers grown by unbalanced magnetron sputtering, Thin Solid Films 493 (2005) 129–134, http://dx.doi.org/10.1016/j.tsf.2005.07.314.

[29] Y. Xu, C.H. Lei, B. Ma, H. Evans, H. Efstathiadis, R. Manisha, M. Massey, U. Balachandran, R. Bhattacharya, Growth of textured MgO through e-beam evaporation and inclined substrate deposition, Supercond. Sci. Technol. 19 (2006) 835–843, http://dx.doi.org/10.1088/0953-2048/19/8/026.

[30] S. Kasap, P. Capper (Eds.), Springer Handbook of Electronic and Photonic Materials, Springer, Cham, 2017, http://dx.doi.org/10.1007/978-3-319-48933-9.

[31] H. Taniguchi, T. Ushiro, Y. Okamoto, Y. Akagi, M. Koba, Influence of preferred orientation in indium tin oxide, MRS Online Proc. Libr. 280 (1992) 523–526, http://dx.doi.org/10.1557/proc-280-523.

[32] D. Mergel, K. Thiele, Z. Qiao, Texture analysis of thin In_2O_3:Sn films prepared by direct-current and radio-frequency magnetron-sputtering, J. Mater. Res. 20 (2005) 2503–2509, http://dx.doi.org/10.1557/jmr.2005.0297.

[33] Y. Chen, Y. Zhou, Q. Zhang, M. Zhu, F. Liu, The correlation between preferred orientation and performance of ITO thin films, J. Mater. Sci. Mater. Electron. 18 (2007) 411–414, http://dx.doi.org/10.1007/s10854-007-9231-7.

[34] F. Paraguay-Delgado, M. Miki-Yoshida, W. Antunez, J. González-Hernández, Y.V. Vorobiev, E. Prokhorov, Morphology and microstructure of textured SnO_2 thin films obtained by spray pyrolysis and their effect on electrical and optical properties, Thin Solid Films 516 (2008) 1104–1111, http://dx.doi.org/10.1016/j.tsf.2007.05.026.

[35] Y.-H. Hu, Y.-C. Chen, H.-J. Xu, H. Gao, W.-H. Jiang, F. Hu, Y.-X. Wang, Texture ZnO thin-films and their application as front electrode in solar cells, Engineering 02 (2010) 973–978, http://dx.doi.org/10.4236/eng.2010.212124.

[36] J.T. Wang, X.L. Shi, W.W. Liu, X.H. Zhong, J.N. Wang, L. Pyrah, K.D. Sanderson, P.M. Ramsey, M. Hirata, K. Tsuri, Influence of preferred orientation on the electrical conductivity of fluorine-doped tin oxide films, Sci. Rep. 4 (2014) 3679, http://dx.doi.org/10.1038/srep03679.

[37] N. Fujimura, T. Nishihara, S. Goto, J. Xu, T. Ito, Control of preferred orientation for ZnO_x films: control of self-texture, J. Cryst. Growth 130 (1993) 269–279, http://dx.doi.org/10.1016/0022-0248(93)90861-p.

[38] M. Wang, L. Jiang, Y. Wang, E.J. Kim, S.H. Hahn, Growth mechanism of preferred crystallite orientation in transparent conducting ZnO:In thin films, J. Am. Ceram. Soc. 98 (2015) 3022–3028, http://dx.doi.org/10.1111/jace.13742.

[39] S. Brahma, P. Jaiswal, K.S. Suresh, K.-Y. Lo, S. Suwas, S.A. Shivashankar, Effect of substrates and surfactants over the evolution of crystallographic texture of nanostructured ZnO thin films deposited through microwave irradiation, Thin Solid Films 593 (2015) 81–90, http://dx.doi.org/10.1016/j.tsf.2015.09.005.

[40] Z. Chen, Y. Zhuo, R. Hu, W. Tu, Y. Pei, B. Fan, C. Wang, G. Wang, Control of morphology and orientation for textured nanocrystalline indium oxide thin film: A growth zone diagram, Mater. Des. 131 (2017) 410–418, http://dx.doi.org/10.1016/j.matdes.2017.06.043.

[41] D. Wan, P. Chen, J. Liang, S. Li, F. Huang, (211)-Orientation preference of transparent conducting In_2O_3:Sn films and its formation mechanism, ACS Appl. Mater. Interfaces 3 (2011) 4751–4755, http://dx.doi.org/10.1021/am2012432.

[42] K. Thiele, S. Sievers, C. Jooss, J. Hoffmann, H.C. Freyhardt, Room-temperature preparation of biaxially textured indium tin oxide thin films with ion-beam-assisted deposition, J. Mater. Res. 18 (2003) 442–447, http://dx.doi.org/10.1557/jmr.2003.0056.

[43] C. Bundesmann, H. Neumann, Tutorial: The systematics of ion beam sputtering for deposition of thin films with tailored properties, J. Appl. Phys. 124 (2018) 231102, http://dx.doi.org/10.1063/1.5054046.

[44] D. Kim, Y. Han, J.-S. Cho, S.-K. Koh, Low temperature deposition of ITO thin films by ion beam sputtering, Thin Solid Films 377–378 (2000) 81–86, http://dx.doi.org/10.1016/s0040-6090(00)01388-2.

[45] Y. Han, D. Kim, J.-S. Cho, S.-K. Koh, Y.S. Song, Tin-doped indium oxide (ITO) film deposition by ion beam sputtering, Sol. Energy Mater. Sol. Cells 65 (2001) 211–218, http://dx.doi.org/10.1016/s0927-0248(00)00097-0.

[46] A. Barranco, A. Borras, A.R. Gonzalez-Elipe, A. Palmero, Perspectives on oblique angle deposition of thin films: From fundamentals to devices, Prog. Mater. Sci. 76 (2016) 59–153, http://dx.doi.org/10.1016/j.pmatsci.2015.06.003.

[47] B. Lacroix, A.J. Santos, S. Hurand, A. Corvisier, F. Paumier, T. Girardeau, F. Maudet, C. Dupeyrat, R. García, F.M. Morales, Nanostructure and physical properties control of indium tin oxide films prepared at room temperature through ion beam sputtering deposition at oblique angles, J. Phys. Chem. C 123 (2019) 14036–14046, http://dx.doi.org/10.1021/acs.jpcc.9b02885.

[48] S. Hurand, A. Corvisier, B. Lacroix, A.J. Santos, F. Maudet, C. Dupeyrat, R. García, F.M. Morales, T. Girardeau, F. Paumier, Anisotropic optical properties of indium tin oxide thin films prepared by ion beam sputtering under oblique angle deposition, Appl. Surf. Sci. 595 (2022) 152945, http://dx.doi.org/10.1016/j.apsusc.2022.152945.

[49] A.J. Santos, B. Lacroix, F. Maudet, F. Paumier, S. Hurand, C. Dupeyrat, V.J. Gómez, D.L. Huffaker, T. Girardeau, R. García, F.M. Morales, Application of advanced (S)TEM methods for the study of nanostructured porous functional surfaces: A few working examples, Mater. Charact. 185 (2022) 111741, http://dx.doi.org/10.1016/j.matchar.2022.111741.

[50] T.P. Rao, M.C. Santhoshkumar, Highly oriented (100) ZnO thin films by spray pyrolysis, Appl. Surf. Sci. 255 (2009) 7212–7215, http://dx.doi.org/10.1016/j.apsusc.2009.03.065.

[51] A.R. Shetty, A. Karimi, M. Cantoni, Effect of deposition angle on the structure and properties of pulsed-DC magnetron sputtered TiAlN thin films, Thin Solid Films 519 (2011) 4262–4270, http://dx.doi.org/10.1016/j.tsf.2011.02.090.

[52] J.-H. Kim, J.-H. Lee, Y.-W. Heo, J.-J. Kim, J.-O. Park, Effects of oxygen partial pressure on the preferential orientation and surface morphology of ITO films grown by RF magnetron sputtering, J. Electroceram. 23 (2009) 169–174, http://dx.doi.org/10.1007/s10832-007-9351-8.

[53] S. Mahieu, Biaxial Alignment in Sputter Deposited Thin Films (Ph.D. thesis), Gent University, 2006, doi: 1854/4836. URL http://hdl.handle.net/1854/LU-468918.

[54] S. Mahieu, G.D. Winter, D. Depla, R.D. Gryse, J. Denul, A model for the development of biaxial alignment in yttria stabilized zirconia layers, deposited by unbalanced magnetron sputtering, Surf. Coat. Technol. 187 (2004) 122–130, http://dx.doi.org/10.1016/j.surfcoat.2004.01.008.

[55] P. Ghekiere, S. Mahieu, R.D. Gryse, D. Depla, Structure evolution of the biaxial alignment in sputter-deposited MgO and Cr, Thin Solid Films 515 (2006) 485–488, http://dx.doi.org/10.1016/j.tsf.2005.12.266.

[56] P. Ghekiere, Structure Evolution of Biaxially Aligned Thin Films Deposited by Sputtering (Ph.D. thesis), Ghent University (Belgium), 2007, doi: 1854/7197.

[57] G. Abadias, F. Anğay, R. Mareus, C. Mastail, Texture and stress evolution in HfN films sputter-deposited at oblique angles, Coatings 9 (2019) 712, http://dx.doi.org/10.3390/coatings9110712.

[58] D.L. Voronov, P. Gawlitza, S. Braun, H.A. Padmore, Spontaneous formation of highly periodic nano-ripples in inclined deposition of Mo/Si multilayers, J. Appl. Phys. 122 (2017) 115303, http://dx.doi.org/10.1063/1.4991377.

[59] P. Agoston, K. Albe, Thermodynamic stability, stoichiometry, and electronic structure of bcc-In_2O_3 surfaces, Phys. Rev. B 84 (2011) 045311, http://dx.doi.org/10.1103/physrevb.84.045311.

[60] R. Balu, A.R. Raju, V. Lakshminarayanan, S. Mohan, Investigations on the influence of process parameters on the structural evolution of ion beam sputter deposited chromium thin films, Mater. Sci. Eng. B: Solid-State Mater. Adv. Technol. 123 (2005) 7–12, http://dx.doi.org/10.1016/j.mseb.2005.06.021.

[61] K. Okamoto, K. Itoh, Incidence angle dependences of columnar grain structure and texture in obliquely deposited iron films, Japan. J. Appl. Phys. 44 (2005) 1382–1388, http://dx.doi.org/10.1143/jjap.44.1382.